SCIENTIFIC REPORTS
nature research

OPEN

Carrier Induced Hopping to Band Conduction in Pentacene

Varsha Rani[1], Pramod Kumar[1], Akanksha Sharma[1], Sarita Yadav[1], Budhi Singh[2], Nirat Ray[1] & Subhasis Ghosh[1*]

Charge transport in organic thin films which are generally polycrystalline is typically limited by the localization of the carriers at lattice defects resulting in low carrier mobilities and carriers move from one state to another state by hopping. However, charge transport in organic semiconductors in their single crystalline phase is coherent due to band conduction and mobilities are not limited by disorder resulting in higher carrier mobility. So it is a challenge to enhance the carrier mobility in a thin film which is the preferred choice for all organic devices. Here, we show that it is possible to increase the carrier mobility in polycrystalline thin films by injecting sufficient carriers such that Fermi level can be moved into the region of high density in Gaussian density of states of molecular solids. When the hopping transport happens through the molecular energy levels whose density is low, mobility is decided by incoherent transport however, when the the hopping transport happens through the energy levels with high density, mobility is decided by coherent transport, as in band conduction. We present results highlighting the observation of both band-like and hopping conduction in polycrystalline organic thin films by varying the concentration of injected charge. More importantly the transition from hopping to band transport is reversible. The observed carrier mobilities in both the regimes match well with theoretical estimates of hopping mobility and band mobility determined from first principles density functional theory.

Low values of charge carrier mobilities in organic thin films is a fundamental issue affecting their applications to integrated circuits, displays and memory devices requiring fast processing[1]. Unlike single crystals where band-like transport is observed[2–5], intrinsic thermal and structural disorder in organic thin films lead to localization of charge carriers in the tail of a Gaussian density of states (GDOS)[6,7] which results due to randomness in positional and energetic disorder in polycrystalline and amorphous thin films. Carriers then need some activation energy to hop between neighboring sites leading to (i) low carrier mobility and (ii) positive temperature coefficient of mobility. The real challenge with polycrystalline organic thin films lies in achieving delocalized band-like conduction resulting in high mobility comparable with that in pure organic single crystals. Although, delocalized charge transport with high mobilities has been observed in pure single crystal[3,5] however, organic single crystals cannot be used in large area rolable and foldable electronic devices. Poor device integration and cross-talk between devices are also the drawbacks of single crystals. Considerable efforts have been put[8,9] towards improving the performance of organic thin films based devices by engineering the growth parameters, substrate/organic interface and device parameters but, high mobilities comparable with that in single crystals could not be achieved. Observation of negative temperature coefficient in polycrystalline thin films have previously been observed and interpreted in terms of large thermal fluctuations in electronic coupling rather than band transport[10–12]. Hence, an understanding of the crossover from localized to delocalized band-like transport in polycrystalline organic thin film is essential. We show that temperature coefficient of mobility can be changed from positive to negative corresponding to a transition from hoping to band-like transport as the Fermi level is modulated by injecting sufficient numbers of carriers. The observed values of carrier mobilities in the band transport regime are two orders of magnitude higher than those in the hoping regime. Our experimental results are supported by theoretical calculations for hoping mobility estimates using Marcus theory[13,14] and density functional theory (DFT) band mobility.

[1]School of Physical Sciences, Jawaharlal Nehru University, New Delhi, 110067, India. [2]Inter-University Accelerator Center, Aruna Asaf Ali Marg, New Delhi, 110067, India. *email: subhasis.ghosh.jnu@gmail.com

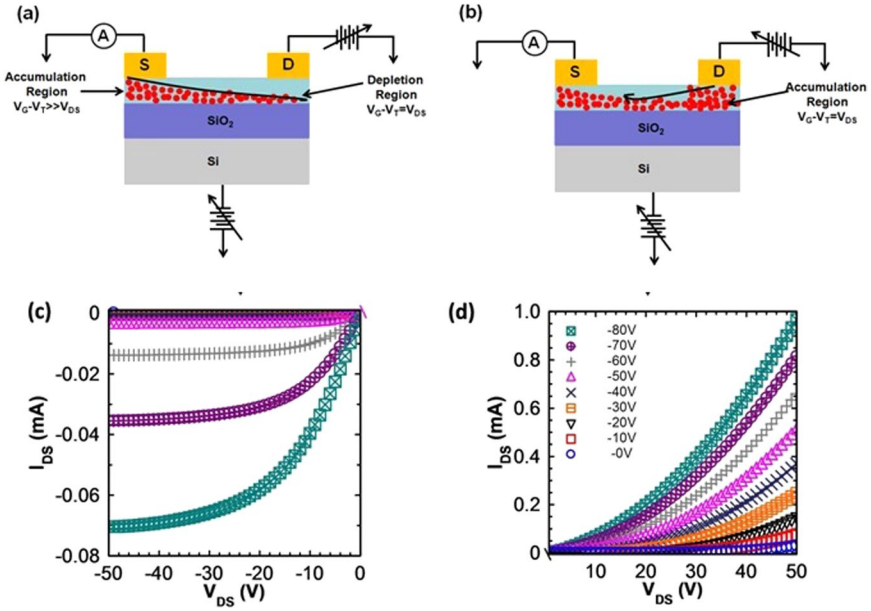

Figure 1. Schematic representation of the working and output characterstics of a p-type OFET: (**a**) Negative V_{DS} regime and (**b**) positive V_{DS} regime. In negative V_{DS} regime, two regions exist within the channel; accumulation region and depletion region. However, in positive V_{DS} regime, there is no depletion region rather only accumulation region exists for the whole channel. (**c**,**d**) Show the room temperature output characteristics ($I_{DS} - V_{DS}$) of pentacene thin film based OFET in negative and positive V_{DS} regime, respectively. Mechanisms of charge transport in negative and positive V_{DS} regime seem different.

Results and Discussion

Figure 1 illustrates the working of a pentacene thin film based organic field effect transistor (OFET) in negative as well as positive source-drain bias (V_{DS}) regime. A negative gate voltage (V_G) accumulates a layer of holes at organic/dielectric interface. When a negative V_{DS} is applied, charge carriers flow from source to drain and two different regions; accumulation region near source and depletion region due to the pinch off the channel near drain exist (schematically show in Fig. 1(a)). However, in positive V_{DS} regime, working of the OFET is different from that in negative V_{DS} regime. When a positive bias is applied at drain, device structure becomes quite similar to a hole only two terminal device (Fig. 1(b)). There are however two key differences; (i) organic thin film is sandwiched laterally between two metal electrodes whereas it is sandwiched vertically in two terminal devices, and (ii) an additional V_G is used to control the density of background charge carriers in the device. In positive V_{DS} regime, as drain is at higher potential than source, holes are injected at the drain electrode and move towards source i.e. source and drain are interchanged. Further, in this regime, as there is no pinch-off, no depletion region is observed within the channel rather only accumulation region exists for the whole channel. Figure 1(c,d) represent the resulting output ($I_{DS} - V_{DS}$) characteristics of pentacene thin film based OFET fabricated under optimized growth conditions (*see* Fig. S1 in Supplementary Information for morphological and structural data), in negative and positive V_{DS} regime, respectively. In negative V_{DS} regime, $I_{DS} - V_{DS}$ exhibits two regions; linear region at small V_{DS} and saturation region at high V_{DS} due to the pinch-off the channel. However, in positive V_{DS} region, as there is no pinch-off, no saturation is observed in $I_{DS} - V_{DS}$ characteristics rather I_{DS} increases non-linearly with V_{DS} (Fig. 1(d)). Further, magnitudes of I_{DS} in positive V_{DS} regime are higher by more than one order in comparison to those in negative V_{DS} regime. I_{DS} increases with V_G in both, negative as well as positive V_{DS} regime due to an increase in density of free holes. The crux of the matter is how to operate OFET so that Fermi level can be sufficiently moved up in the high density of states region from the region with low density of states in GDOS.

Figure 2(a) shows the I_{DS} as a function of the negative $|V_{DS}|$ on a log-log plot. Two regions; linear and saturation are observed clearly in $I_{DS} - V_{DS}$. We estimate the field-effect mobility, μ, by fitting the $I_{DS} - V_{DS}$ characteristics in the linear region as[15]: $I_{DS} = \mu \frac{W}{L} C_i \left[(V_G - V_T) V_{DS} - \frac{V_{DS}^2}{2} \right]$, where C_i is the dielectric capacitance per unit area and V_T is the threshold voltage. The room temperature mobility has been found to be 0.3 cm^2/Vs which is at least two order of magnitude lower than that in single crystalline pentacene, matching well with the typical mobilities observed in other studies[16–19]. Figure 2(b) shows the variation of the extracted carrier mobilities with temperature and V_G. We find that at all V_G, mobilities increase with temperature exhibiting Arrhenius behavior ($\mu \sim exp(-E_a/k_BT)$, E_a being the activation energy, k_B, Boltzmann's constant and T, the temperature). This is consistent with thermally activated hopping transport. Inset of Fig. 2(b) shows that at higher V_G, charge carriers require lesser activation energy to hop to neighboring sites. This is attributed to the filling of the higher energy states by additional charge carriers at high V_G. In other words, Fermi level shifts from the tail towards the center of the GDOS. Next, we compare the experimentally extracted hopping mobility with that estimated theoretically using Marcus theory[13]. Within this approach, the charge transfer between neighboring molecular sites is

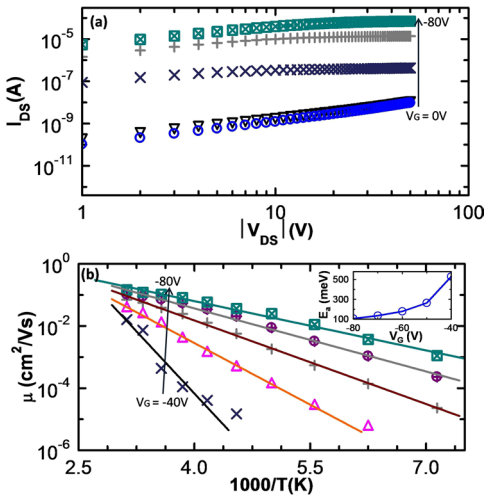

Figure 2. Negative source−drain regime: (**a**) $I_{DS} - V_{DS}$ on a log-log plot for a pentacene thin film based OFET. Here, linear and saturation regions are clearly distinguishable. (**b**) Arrhenius temperature dependence of charge carrier mobility measured at different V_G. Inset shows the variation of activation energy with the V_G. Different symbols represent different values of the applied V_G.

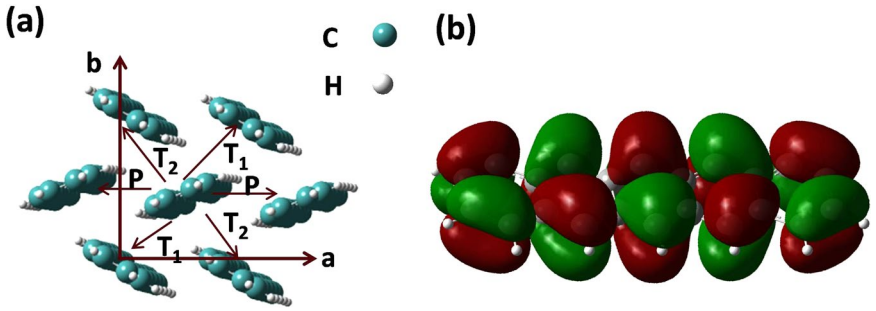

Figure 3. Dimer representation: (**a**) Schematic representation of different dimers in ab-plane; *P* dimers along a-axis, T_1 and T_2, transverse dimers along diagonals and (**b**) isosurface representing the charge density distribution on HOMO of pentacene.

described as a self-exchange reaction process. First diffusion coefficient, (D) is calculated using the charge transfer rate (k_{ij}) as[20]

$$D = \frac{1}{2n}\sum_j r_j^2 k_{ij} P_j; \;\; k_{ij} = \frac{4\pi^2}{h} t_{ij}^2 \frac{\exp(-\lambda/4k_B T)}{\sqrt{4\pi\lambda k_B T}} \tag{1}$$

and then hopping mobility is estimated using the Einstein relation as,

$$\mu = \frac{eD}{k_B T} \tag{2}$$

where, n is the space dimensionality, r_j, hopping distance, e, the electronic charge, h, the Planck's constant, $P_j(=k_{ij}/\sum k_{ij})$ is hopping probability of a charge carrier corresponding to the hopping pathway, j, the transfer integral, t_{ij} represents the strength of the coupling between neighboring sites, i and j and λ, the intramolecular reorganization energy arises due to the relaxation of the geometry of a molecule during charge transfer. This is estimated by carrying out single point energy calculations on optimized geometries of neutral and ionic molecule as[21] $\lambda = [(E_{\pm}^{'} - E_{\pm}) + (E^{'} - E)]$. Here E and $E_{\pm}$ are the ground state energies of the molecule in the neutral state and in the ionic state ('+' and '−' signs represent the cation and anion, respectively) respectively. $E^{'}$ is the energy of the neutral molecule in the optimized geometry of the charged molecule and $E_{\pm}^{'}$ is the energy of the charged molecule in the optimized geometry of the neutral molecule. t_{ij} have been estimated by employing dimer projection method[22], directly from the orbitals of dimers and monomers. Values of λ, t_{ij} and μ calculated in this way are found to be; $\lambda = 97$ meV, t_{ij} for different dimers lying in ab-plane Fig. 3(a)), *i.e.*, *P*, T_1 and $T_2 = 57.74$, 65.38 and 68.46 meV, and $\mu = 1.8\,\text{cm}^2/\text{Vs}$. Figure 3(b) shows the distribution of charge density on the highest occupied molecular orbital (HOMO) of pentacene. We observe that HOMO is uniformly distributed over the all the

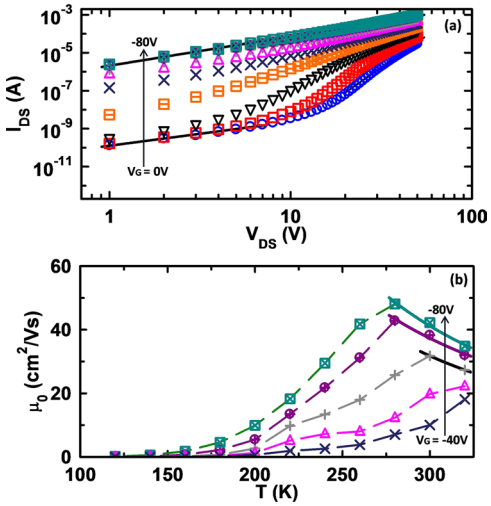

Figure 4. Positive drain – source regime: (**a**) $I_{DS} - V_{DS}$ on a log-log plot for a pentacene thin film based OFET. $V_{DS} - I_{DS}$ characteristics are similar to two terminal devices *i.e.* initial Ohmic region and then field dependent SCLC. However as V_G increases SCLC starts weakening and approaches Ohmic region for the entire range of V_{DS}. (**b**) Temperature dependence of charge carrier mobility measured at different V_G in positive V_{DS} regime. Dashed lines are used to connect the different data points at same V_G and solid lines represent fitting according to the power-law ($\mu(T) \sim T^{-\gamma}$) at high temperatures. Different colored symbols represent different values of the V_G.

benzene rings in pentacene. Further, as H-atoms have no p-orbitals, they do not contribute to the π-orbitals of HOMO. Predicted magnitudes of λ, t_{ij} and μ are comparable with that estimated in previous studies on pentacene[23–25]. The theoretically calculated mobility estimates are higher than the experimentally observed values. This can be attributed to the thermal and energetic disorder in neighboring molecules that have not been included in theoretical model.

It can be emphasized here that this should be the highest mobility that can be achieved in hopping regime in a-b plane whereas along c-axis maximum mobility has been found to be $4.45 \times 10^{-5} cm^2/Vs$. Actually, c-axis should be the relevant direction for charge transport in two-terminal sandwiched devices. For comparison, we also studied Al/pentacene/Au based two terminal devices (For details, see Figs. S2 and S3 in Supplementary Information). Mobilities in these devices have been estimated using space charge limited conduction (SCLC) method[6] and found to be $1.21 \times 10^{-5} cm^2/Vs$, close to the theoretically predicted value. This can be attributed to the minimal effect of disorder on transport along c-axis compared to that in a-b plane as evident from the excellent matching of experimental and theoretical values of mobility along c-axis compared to difference (0.3 vs 1.8 cm^2/Vs) in a-b plane.

Figure 4(a) shows the I_{DS} as a function of positive V_{DS}, on a log-log plot. We observe that magnitudes of current in this regime are higher by more than one order of magnitude than those in negative V_{DS} regime. At low V_{DS}, the carriers injected from one electrode redistribute themselves in such a way that they replace the holes flowing out at the other end. Hence charge transport is contact limited in which I_{DS} is governed by the thermally generated free charge carriers in the device and varies linearly with V_{DS} resulting in an ohmic region. At high bias, the injected carrier density becomes large resulting in accumulation of holes, which create a space charge region. The current then shows non-linear behavior with V_{DS} consistent with space charge limited conduction (SCLC)[6]. As expected, no saturation in current is observed because channel is not pinched-off in this regime and hence, no depletion region forms.

With increasing V_G, the background charge carrier concentration in the device increases. At higher V_Gs, more carriers are injected from the source. This weakens the SCLC due to enhanced conduction through the channel. Thus SCLC weakens and eventually a crossover to ohmic conduction is observed, as shown in Fig. 4(a). As the output characteristics of the device in this regime are different from those in negative V_{DS} regime hence, conventional transistor method cannot be applied to extract mobility. $I_{DS} - V_{DS}$ characteristics shown in Fig. 4(a) have been simulated by solving the set of equations, $I_{DS} = ep(x)\mu[T,\ F]F(x)A$, $dF(x)/dx = ep(x)/\varepsilon_s$ and $V_{DS} = \int_0^L F(x)dx$, self consistently. The same simulation has been used to extract the mobility in two-terminal devices and as mentioned before, excellent corroboration of experimental data with first principle theoretical data is observed. Here A is the effective area of cross-section, ε_s is the dielectric constant of organic semiconductor and $p(x)$ is the density of charge carriers at a distance x from the injecting electrode. Room temperature mobility estimated in this way has been found to be 48.3 cm^2/Vs at a V_G of -80 V which is almost two orders of magnitude higher than that in the negative V_{DS} regime and also much higher than the hopping mobility limit set by Marcus theory. And the most importantly this value is close to mobiilities generally obtained in pentacene single crystal[3].

Figure 4(b) shows the variation of μ with temperature and V_G, estimated in positive V_{DS} regime. We observe that mobilities increase with temperature up to ~280 K, consistent with charge transport limited by impurity scattering[15,26]. Beyond ~280 K, the decrease in mobility with an increase in temperature can be explained on the

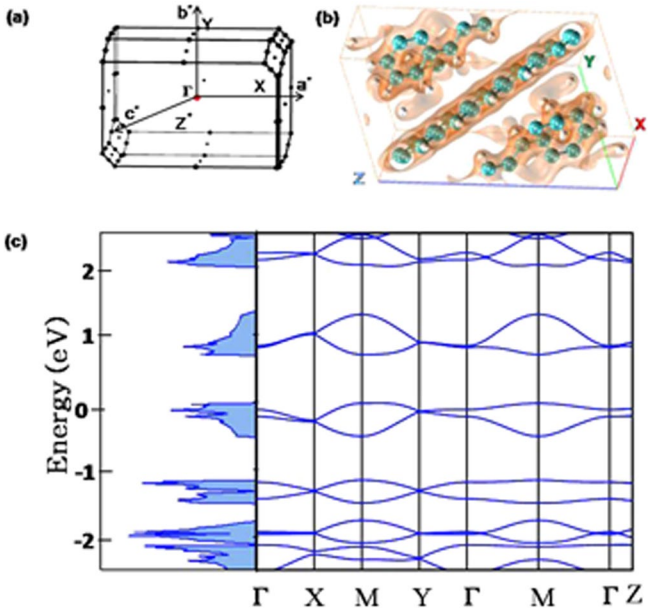

Figure 5. Density functional theory calculations: (**a**) First Brillouin zone for crystal structure of pentacene in reciprocal lattice. (**b**) Distribution of charge density in the surrounding of molecules in pentacene unit cell. (**c**) Calculated band structure and density of states of pentacene using periodic DFT calculations. Different high symmetry points are represented in units of $(2\pi/a, 2\pi/b, 2\pi/c)$ along certain directions as $\Gamma = (0, 0, 0)$, $X = (0.5, 0, 0)$, $M = (0.5, 0.5, 0)$, $Y = (0, 0.5, 0)$ and $Z = (0, 0, 0.5)$. Zero of energy has been set at the valence band maximum.

basis of phonon scattering[15,26]. After fitting the mobility curves in the high temperature range according to $\mu(T) \sim T^{-\gamma}$, γ has been found to be in the range of 2.1–2.4. These values of γ match well with those obtained for pure organic crystals[2,27], further emphasizing the role of phonon scattering in polycrystalline organic thin films. The role of thermal fluctuations in intermolecular electronic coupling as suggested by *Troisi et al.*[10] is ruled out by carrying out molecular dynamics simulations. We observe no signature of band-like transport from these simulations.

Further, as mentioned before, the room temperature mobility estimated from $I_{DS} - V_{DS}$ in positive V_{DS} regime is consistent with the band mobility values expected for single crystals[3]. To support our experimental observations of band transport, we have theoretically estimated the band mobilities of pentacene bulk phase[28,29] using periodic DFT based calculations. Brillouin zone of pentacene with high symmetric *k*-points used in the calculation of band structure are shown in Fig. 5(a). Figure 5(b) shows the distribution of charge density in the surrounding of molecules in pentacene unit cell. Figure 5(c) shows the band structure and density of states for pentacene bulk phase[29]. The band structure calculations have been carried out in Brillouin zone connecting the different high symmetry points, X, M, Y, Z with the internal coordinates being (0, 0, 0), (0.5, 0, 0), (0.5, 0.5, 0), (0, 0.5, 0) and (0, 0, 0.5) in units of $(2\pi/a; 2\pi/b; 2\pi/c)$, respectively. As there are two molecules in equivalent configuration in pentacee unit cell, each band in band structure is composed of two subbands. Pentacene shows a direct band gap at Γ to be 0.70 eV which is lower than the experimentally observed one (2.2 eV)[30]. This is a common drawback of DFT however, it does not affect the accuracy of transport parameters estimated from band structure because, transport parameters are estimated from the slope of the valence or conduction band and not from the band gap.

From band structure, carrier mobility can be estimated as[24],

$$\mu = \frac{e\tau}{m_e} \tag{3}$$

so there are two main parameters to be determined; effective mass (m_e) and relaxation time (τ). Effective mass has been calculated from band structure as[24], $m_e = \hbar^2\left(\frac{d^2E(k)}{dk^2}\right)^{-1}$. The relaxation time has been estimated using the acoustic deformation potential and follows as[31],

$$\tau = \frac{\hbar^2 B}{(2\pi k_B T)^{1/2} m^{1/2} D_p} \tag{4}$$

where B is the bulk modulus and D_p is the accoustic deformation potential. B and D_p can be given by[31],

$$B = V_0\left(\frac{\partial^2 E}{\partial V^2}\right)_{V_0} \tag{5}$$

V_0 being the equilibrium volume of the unit cell and

$$D_p = \frac{1}{V_0}\frac{\partial E_{VC}}{\partial(\Delta V)} \tag{6}$$

where ΔV represents the change in the volume of pentacene unit cell and E_{vc} is the energy difference between the core level and top of maximum valence band for hole transport. As localized 1 s level is not sensitive to the slight lattice deformation, it can be used as energy reference to obtain the absolute band energy change for valence band maximum (VBM). This energy difference between the VBM and 1 s level is plotted against the fractional change in volume to obtain D_p. Then band mobility, estimated using Eq. 3 has been found to be 55.52 cm^2/Vs which is higher than our experimental value (48.34 cm^2/Vs). The difference in experimental and theoretical values can be accounted if structural disorder is included in the calculation, which is extremely difficult and beyond the scope of present problem.

Our results then suggest that the crossover from hopping to band-like transport occurs due to the large variation in the injected carrier concentration in negative and positive V_{DS} regime. To confirm this, we have analytically estimated the carrier concentration and corresponding Fermi level in both regimes. The total charge concentration in the channel at a spatial position x (distance from the injecting electrode) can be written as:

$$p_{tot}(x) = p_f + p_G + p_{DS}(x) \tag{7}$$

where p_f is the concentration of thermally generated free charge carriers and p_G and $p_{DS}(x)$ are the charge carrier concentrations injected by the gate and V_{DS}, respectively. In the negative V_{DS} regime, when V_G is larger than the V_{DS}, p_{tot}, using gradual channel approximation can be written as[32],

$$p_{tot}(x) = p_f + C_i\left(V_G - \frac{x}{L}V_{DS}\right)/et \tag{8}$$

where t is the thickness of the accumulation layer and has been take to be 10 nm. When V_{DS} approaches the V_G, channel is depleted and the Fermi level lies in the deep localized states below the equilibrium level ($-\sigma^2/k_BT$, σ being the width of GDOS), resulting into low values of mobility[6].

In the positive V_{DS} regime, at low bias, injected carrier concentration is equal to the extracted one and the transport is injection limited. Then total carrier concentration and position of the Fermi level is decided by the V_G i.e.

$$p_{tot} = p_0 + C_iV_G/et \tag{9}$$

At high bias, all the charge carriers injecting at one electrode are not balanced by those extracting at the other, resulting accumulation of charge carriers (SCLC). Then $p_{DS}(x)$ can be expressed as (see Supplementary Information S4)[15,33],

$$p_{DS}(x) = 3V_{DS}\varepsilon_s x^{-1/2}/4L^{3/2} \tag{10}$$

and the total carrier concentration is given by Eq. 7. Dependence of the Fermi level on the carrier concentration is given by[7],

$$\int_{-\infty}^{\infty} f(E, E_F)g(E)dE = p_{tot} \tag{11}$$

where $f(E, E_F) = [1 + \exp(E_F - E)/k_BT]^{-1}$, is Fermi function, exhibiting the energetic distribution of the charge carriers at thermal equilibrium. $g(E)$ represents the GDOS in HOMO of the organic semiconductor given by[7],

$$g(E) = (N_V/\sqrt{2\pi}\sigma)\ exp\left(-\frac{E^2}{2\sigma^2}\right) \tag{12}$$

N_V is effective density of states in the HOMO. Hence, position of E_F depends on three parameters; (i) spatial position (x) between source and drain (ii) magnitude of negative or positive V_{DS} i.e. $|V_{DS}|$ and (iii) magnitude of V_G. Lets examine the effect of each of these parameters separately.

Estimated positions of Fermi level in negative and positive V_{DS} regime have been represented in Fig. 6. In the negative V_{DS} regime, the Fermi level goes down and becomes flat after the channel is pinched-off. Hence there are two regions in negative V_{DS} regime: accumulation and depletion. The density of occupied states is high in the accumulation region and low in the depletion region, resulting in the current being controlled by the low mobility region i.e. the tail of the GDOS. In the positive V_{DS} regime, as there is no depletion region, the Fermi level across the entire channel remains near the center of the GDOS and the current is governed by the high mobility region (see Figs. S4 and S5 in Supplementary Information). This would explain the band-like transport with higher mobilities in positive V_{DS} regime in pentacene thin film based OFETs. Figure 7 schematically illustrates the charge transport, governed by two different sections of the GDOS. When the Fermi level lies near the tail of the GDOS, transport is described by thermally activated hopping. As the Fermi level moves towards the central region, band-like transport becomes possible. Table 1 summarizes the mobilities obtained in two-terminal and three-terminal devices. we observe that mobilities in two-terminal devices are lower by several orders of magnitude than those obtained in three-terminal devices. This large difference in mobilities in different device configuration is attributed to the anisotropy in the coupling between the dimers along different axis.

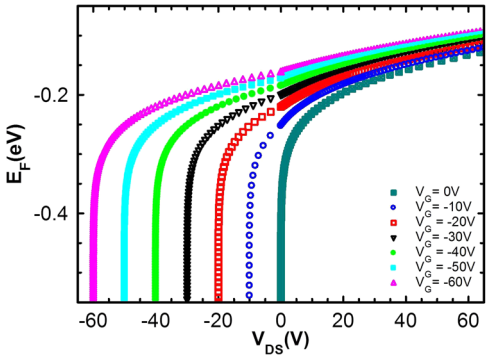

Figure 6. Estimated positions of Fermi-energy level: Estimated Fermi level (E_F) as a function of V_{DS} at different $|V_G|$.

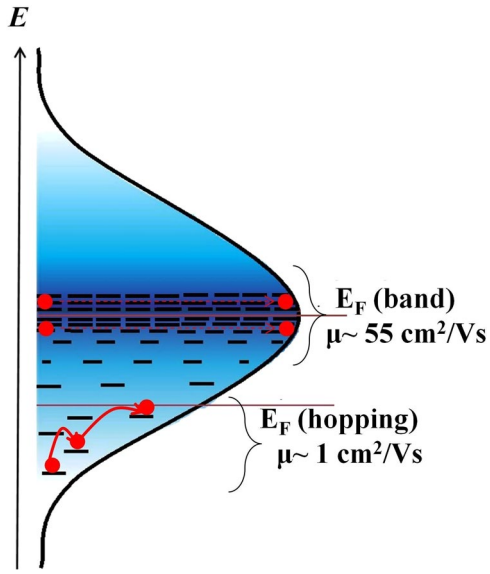

Figure 7. Schematic representation of charge transport in GDOS: Schematic illustration of charge transport governed by two different sections of the GDOS. When the Fermi level lies near the tail of the GDOS, transport is described by thermally activated hopping. As the Fermi level moves towards the central region, band-like transport becomes possible.

		μ_{exp} (cm^2/Vs)	μ_{th} (cm^2/Vs)	Mechanism of charge transport
2T		1.21×10^{-5}	4.45×10^{-5}	Hopping
3T	−ve *VDS*	0.32	1.84	Hopping
(OFET)	+ve V_{DS}	48.34	55.52	Band

Table 1. Summary of experimentally observed mobility (μ_{exp}) and theoretically estimated mobility (μ_{th}) in two-terminal (2T) and three-terminal (3T) devices.

In conclusion, we have shown that both, hopping and band-like transport can be achieved in same organic system by varying the concentration of injecting carriers. This has been achieved by exploiting the presence and absence of pinch-off region by changing the polarity of source and drain in FETs. Band-like conduction associated with high mobility has been observed in positive V_{DS} regime due to the high concentration of injected carriers which moves the Fermi level near the center of the GDOS. Here, density of localized states is so high that charge carriers require negligible activation energy to move to neighboring sites and act like a wave, resulting in band-like transport. It is then also conceivable that this approach can possibly be used to access high mobility regimes in the broader class of disordered semiconductors and insulators.

Methods

Experimental details. We choose pentacene for our study, due to its relatively high carrier mobility in polycrystalline thin film and single crystal form[3,14]. High purity (>99.999%), triple sublimed pentacene has been thermally evaporated to grow thin films. For two terminal devices, 200 nm single layer of pentacene is sandwiched between Al and Au. We fabricate three terminal OFETs with Au source, drain contacts on a 100 nm thick pentacene film grown on n^{++} Si/SiO_2 substrate. All the thin films have been grown at a base pressure of 5×10^{-6} mbar with an extremely low evaporation rate of 0.1 Å/s to minimize structural disorder[9]. The channel length, L and width, W are fixed at 20 μm and 3 mm, respectively.

Computational details. Theoretical estimates for the hopping mobility have been calculated using Gaussian 09[34], by employing ground state energy calculations on pentacene monomer and dimers using a B3LYP (Becke, three-parameter, Lee-Yang-Parr) functional[35,36] and 631-G (d, p) basis set[37]. Transfer integrals are calculated using versatile Object-oriented Toolkit for Coarse-graining Applications (VOTCA) package[38,39]. We take into account the non-orthonormality of frontier orbitals of monomers and estimate the transfer integrals by projecting monomer orbitals on the dimer orbitals[22]. We estimate the band mobility using periodic DFT calculations using Quantum Espresso package[40], within the generalized gradient approximation with Perdew-Burke-Ernzerhol (PBE)[41] exchange correlation function and ultrasoft pseudopotentials. Dispersion interactions between organic molecules are taken into account by using London type pairwise empirical atomic interactions as implemented by DFT-D2 method[42,43].

Received: 27 September 2019; Accepted: 25 November 2019;
Published online: 27 December 2019

References

1. Ruiz, C., García-Frutos, E. M., Hennrich, G. & Gómez-Lor, B. Organic semiconductors toward electronic devices: high mobility and easy processability. *J. Phys. Chem. Lett.* **3**, 1428–1436 (2012).
2. Gershenson, M., Podzorov, V. & Morpurgo, A. Colloquium: Electronic transport in single-crystal organic transistors. *Rev. Mod. Phys.* **78**, 973 (2006).
3. Jurchescu, O. D., Baas, J. & Palstra, T. T. M. Effect of impurities on the mobility of single crystal pentacene. *Appl. Phys. Lett.* **84**, 3061–3063 (2004).
4. Krupskaya, Y., Gibertini, M., Marzari, N. & Morpurgo, A. F. Band-like electron transport with record-high mobility in the tcnq family. *Adv. Mater.* **27**, 2453–2458 (2015).
5. Podzorov, V. *et al*. Intrinsic charge transport on the surface of organic semiconductors. *Phys. Rev. Lett.* **93**, 086602 (2004).
6. Bässler, H. Charge transport in disordered organic photoconductors a monte carlo simulation study. *phys. status solidi (b)* **175**, 15–56 (1993).
7. Baranovskii, S. D. Theoretical description of charge transport in disordered organic semiconductors. *phys. status solidi (b)* **251**, 487–525 (2014).
8. Boudinet, D. *et al*. Influence of substrate surface chemistry on the performance of top-gate organic thin-film transistors. *J. Am. Chem. Soc.* **133**, 9968–9971 (2011).
9. Kumar, P., Sharma, A., Yadav, S. & Ghosh, S. Morphology optimization for achieving air stable and high performance organic field effect transistors. *Org. Electron.* **14**, 1663–1672 (2013).
10. Troisi, A. & Orlandi, G. Charge-transport regime of crystalline organic semiconductors: Diffusion limited by thermal off-diagonal electronic disorder. *Phys. Rev. Lett.* **96**, 086601 (2006).
11. Fratini, S. & Ciuchi, S. Bandlike motion and mobility saturation in organic molecular semiconductors. *Phys. Rev. Lett.* **103**, 266601 (2009).
12. Sakanoue, T. & Sirringhaus, H. Band-like temperature dependence of mobility in a solution-processed organic semiconductor. *Nat. Mater.* **9**, 736–740 (2010).
13. Marcus, R. A. Electron transfer reactions in chemistry. theory and experiment. *Rev. Mod. Phys.* **65**, 599–610 (1993).
14. Afzali, A., Dimitrakopoulos, C. D. & Breen, T. L. High-performance, solution-processed organic thin film transistors from a novel pentacene precursor. *J. Am. Chem. Soc.* **124**, 8812–8813 (2002).
15. Sze, S. M. & Ng., K. K. *Physics of Semioconductor Devices, 3rd edition*. (Wiley-Interscience, 2006).
16. Chen, C.-M., Liu, C.-M., Tsai, M.-C., Chen, H.-C. & Wei, K.-H. A nanostructured micellar diblock copolymer layer affects the memory characteristics and packing of pentacene molecules in non-volatile organic field-effect transistor memory devices. *J. Mater. Chem. C* **1**, 2328–2337 (2013).
17. Na, J. H., Kitamura, M., Lee, D. & Arakawa, Y. High performance flexible pentacene thin-film transistors fabricated on titanium silicon oxide gate dielectrics. *Appl. Phys. Lett.* **90**, 163514 (2007).
18. Chou, W.-Y. *et al*. Effect of surface free energy in gate dielectric in pentacene thin-film transistors. *Appl. Phys. Lett.* **89**, 112126 (2006).
19. Fritz, S. E., Kelley, T. W. & Frisbie, C. D. Effect of dielectric roughness on performance of pentacene tfts and restoration of performance with a polymeric smoothing layer. *J. Phys. Chem. B* **109**, 10574–10577 (2005).
20. Hutchison, G. R., Ratner, M. A. & Marks, T. J. Intermolecular charge transfer between heterocyclic oligomers. effects of heteroatom and molecular packing on hopping transport in organic semiconductors. *J. Am. Chem. Soc.* **127**, 16866–16881 (2005).
21. Deng, W.-Q. & Goddard, W. A. I. Predictions of hole mobilities in oligoacene organic semiconductors from quantum mechanical calculations. *J. Phys. Chem. B* **108**, 8614–8621 (2004).
22. Baumeier, B., Kirkpatrick, J. & Andrienko, D. Density-functional based determination of intermolecular charge transfer properties for large-scale morphologies. *Phys. Chem. Chem. Phys.* **12**, 11103–11113 (2010).
23. Yavuz, I., Martin, B. N., Park, J. & Houk, K. N. Theoretical study of the molecular ordering, paracrystallinity, and charge mobilities of oligomers in different crystalline phases. *J. Am. Chem. Soc.* **137**, 2856–2866 (2015).
24. Kobayashi, H. *et al*. Hopping and band mobilities of pentacene, rubrene, and 2,7-dioctyl[1]benzothieno[3,2-b][1]benzothiophene (c8-btbt) from first principle calculations. *J. Chem. Phys.* **139**, 014707 (2013).
25. Nguyen, T. P., Shim, J. H. & Lee, J. Y. Density functional theory studies of hole mobility in picene and pentacene crystals. *J. Phys. Chem. C* **119**, 11301–11310 (2015).
26. Kasap, S. O. *Principles of electronic materials and devices* (McGraw-Hill, 2006).
27. Heck, A., Kranz, J. J. & Elstner, M. Simulation of temperature-dependent charge transport in organic semiconductors with various degrees of disorder. *J. Chem. Theory Comput.* **12**, 3087–3096 (2016).

28. Götzen, J., Käfer, D., Wöll, C. & Witte, G. Growth and structure of pentacene films on graphite: Weak adhesion as a key for epitaxial film growth. *Phys. Rev. B* **81**, 085440 (2010).
29. Campbell, R. B., Robertson, J. M. & Trotter, J. The crystal structure of hexacene, and a revision of the crystallographic data for tetracene. *Acta Crystallogr.* **15**, 289–290 (1962).
30. Brehmer, L. Organic molecular crystals. their electronic states. van e. a. silinsh. springer series in solid state sciences, vol. 16. 1. auflage. berlin/heidelberg/new york: Springer verlag 1980. 389 s., geb., dm 92.—. *Acta Polym.* **32**, 665–665 (1981).
31. Wang, D., Shi, W., Chen, J., Xi, J. & Shuai, Z. Modeling thermoelectric transport in organic materials. *Phys. Chem. Chem. Phys.* **14**, 16505–16520 (2012).
32. Weis, M. Gradual channel approximation models for organic field-effect transistors: The space-charge field effect. *J. Appl. Phys.* **111**, 054506 (2012).
33. Zhu, Y. B. & Ang, L. K. Analytical re-derivation of space charge limited current in solids using capacitor model. *J. Appl. Phys.* **110**, 094514 (2011).
34. Frisch, M. J. *et al. Gaussian 09 (Revision A02)* (2009).
35. Becke, A. D. Density-functional exchange-energy approximation with correct asymptotic behavior. *Phys. Rev. A* **38**, 3098–3100 (1988).
36. Lee, C., Yang, W. & Parr, R. G. Development of the colle-salvetti correlation-energy formula into a functional of the electron density. *Phys. Rev. B* **37**, 785–789 (1988).
37. Rassolov, V. A., Pople, J. A., Ratner, M. A. & Windus, T. L. 6-31g* basis set for atoms k through zn. *J. Chem. Phys.* **109**, 1223–1229 (1998).
38. Rühle, V., Junghans, C., Lukyanov, A., Kremer, K. & Andrienko, D. Versatile object-oriented toolkit for coarse-graining applications. *J. Chem. Theory Comput.* **5**, 3211–3223 (2009).
39. Ruhle, V. *et al.* Microscopic simulations of charge transport in disordered organic semiconductors. *J. Chem. Theory Comput.* **7**, 3335–3345 (2011).
40. Giannozzi, P. *et al.* Quantum espresso: a modular and open-source software project for quantum simulations of materials. *J. Phys.: Condens. Matter* **21**, 395502 (2009).
41. Perdew, J. P., Burke, K. & Ernzerhof, M. Generalized gradient approximation made simple. *Phys. Rev. Lett.* **78**, 1396–1396 (1997).
42. Grimme, S. Semiempirical gga-type density functional constructed with a long-range dispersion correction. *J. Comput. Chem.* **27**, 1787–1799 (2006).
43. Grimme, S., Antony, J., Ehrlich, S. & Krieg, H. A consistent and accurate ab initio parametrization of density functional dispersion correction (dft-d) for the 94 elements h-pu. *J. Chem. Phys.* **132**, 154104 (2010).

Acknowledgements

V.R. and A.S. thank UGC and CSIR, India, respectively for the financial support through fellowship. This work was partly supported by DST PURSE, Government of India.

Author contributions

S.G. conceived the idea and designed the research. V.R., P.K., A.S. and S.Y. fabricated devices and performed experiments (equal contribution). V.R. and N.R. simulated experimental data and performed theoretical calculations. S.G. supervised all the investigations. V.R., B.S. and N.R. wrote the manuscript under the supervision of S.G.

Competing interests

The authors declare no competing interests.

Additional information

Supplementary information is available for this paper at https://doi.org/10.1038/s41598-019-56558-w.

Correspondence and requests for materials should be addressed to S.G.

Reprints and permissions information is available at www.nature.com/reprints.

Publisher's note Springer Nature remains neutral with regard to jurisdictional claims in published maps and institutional affiliations.